Electrical and Computer Engineering Faculty Research & Creative Works

Electrical and Computer Engineering

15 May 2005

AC Impedance Measurement Techniques

Keith Corzine
Missouri University of Science and Technology

M. Belkhayat

Yakov L. Familiant

Jing Huang

Ac Impedance Measurement Techniques

Y.L. Familiant, K.A. Corzine, J. Huang, and M. Belkhayat [†]

University of Missouri - Rolla
1870 Miner Circle
Rolla, MO 65401

[†] Newport News Shipbuilding
4101 Washington Avenue
Newport News, VA 23607

Abstract - **Naval ship as well as aerospace power systems are incorporating a greater degree of power electronic switching sources and loads. Although these power electronics based components provide exceptional performance, they are prone to instability due to their high efficiency and constant power characteristics which lead to negative impedance. When designing these systems, integrators must consider the impedance versus frequency at a system interface (which designates source and load). Stability criterions have been developed in terms of source and load impedance for both dc and ac systems and it is often helpful to have techniques for impedance measurement. For dc systems, the measurement techniques have been well established. This paper suggests several methods for measuring ac impedance including utilization of power converters, induction machines and chopper circuits. Simulation results on an example ac system demonstrate the effectiveness of the proposed methods.**

I. INTRODUCTION

Power electronic based systems are prone to negative impedance instability due to the constant-power nature of the individual components [1-5]. Previous research has shown that the instabilities can be avoided in some systems by modification of the power electronic controls [2]. Other research has defined admittance space criteria based on a dc interface which can be used to design system components [3]. Recent research has shown that stability criteria for ac systems can be developed based on the *q-d* impedances of the source and load (defined at a particular system interface) [4]. Along these lines, a method of ac impedance measurement was proposed which is based on series injection of perturbation voltages [5]. This paper suggests additional ac

impedance measurement techniques which are based on shunt current injection. In particular, two types of power converters are proposed for current injection as well as a wound rotor induction machine.

II. CONSTANT-POWER LOAD SYSTEM

A. System Description

Figure 1 shows the example system used to illustrate impedance measurement concepts. For simplicity, a fixed-frequency ac power source with input inductors is used to represent a utility grid or a synchronous generator. The source is connected to a full-bridge IGBT rectifier through an input R-L-C filter; the purpose of which is to eliminate PWM frequency switching harmonics from voltages at the source terminals. Constant power load performance is achieved by keeping the dc bus voltage v_{dc} constant across the constant resistance r_{load}. The rectifier control also maintains unity power factor at the source terminals (*a-b-c*). Table I contains a list of parameters and operating conditions used in the example system.

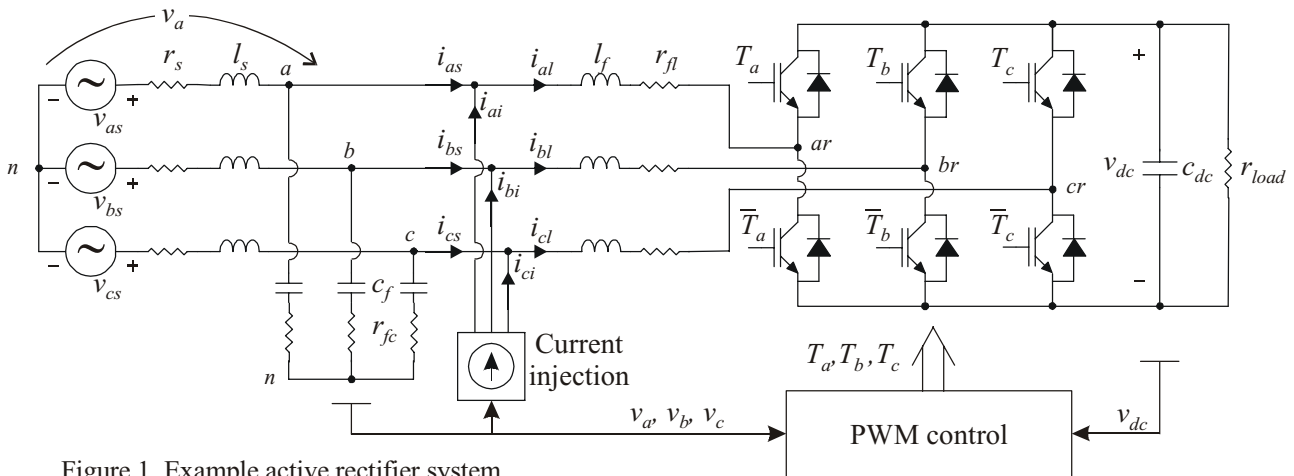| Table I. Example system parameters.		
$r_s = 0.01\,\Omega$	$l_s = 0.4\,\text{mH}$	$r_r = 0.01\,\Omega$
$r_f = 18.9\,\Omega$	$l_f = 1\,\text{mH}$	$c_f = 2.81\,\mu\text{F}$
$r_{load} = 67.6\,\Omega$	$c_{dc} = 3300\,\mu\text{F}$	
$v_{dc}^* = 500\,\text{V}$	$v_s = 133\,\text{V}$	$f_e = 60\,\text{Hz}$

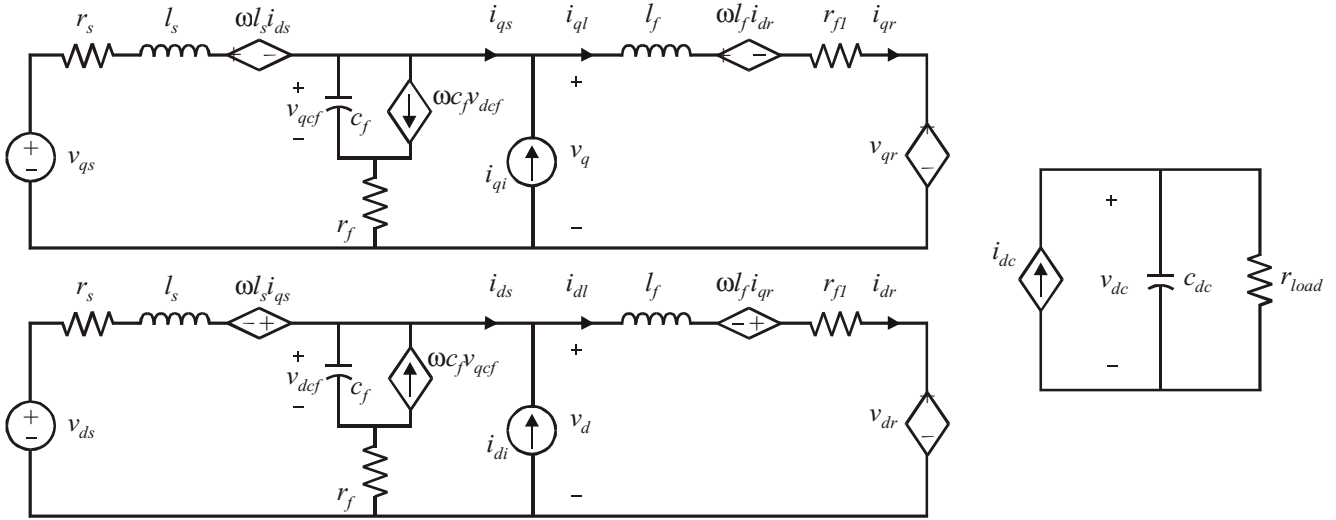Figure 1. Example active rectifier system.

Figure 2. Example system in the arbitrary reference frame.

Where v_{dc}^* is the commanded dc voltage, f_e is the source frequency, and v_s is the rms value of the source voltages v_{as}, v_{bs}, and v_{cs}. Also shown in Figure 1 is the current injection. This is not a part of the system, but will be utilized later to induce small current disturbances to obtain the source impedance and load admittance. Figure 2 shows the rectifier system in the arbitrary q-d reference frame. The average-value models described below rely on a combination of the source reference frame (aligned so that $v_{ds}^e = 0$) and machine variables. The rectifier control is formulated in the synchronous reference frame (aligned so that $v_d^s = 0$) and can be described in this way. Considering the real and reactive power into the rectifier load in the synchronous reference frame which is

$$P_e = \frac{3}{2}\left(v_q^e i_{ql}^e + v_d^e i_{dl}^e\right) \qquad (1)$$

$$Q_e = \frac{3}{2}\left(v_q^e i_{dl}^e - v_d^e i_{ql}^e\right) \qquad (2)$$

Since $v_d^s = 0$ in this reference frame, unity power factor (at the a-b-c terminals) can be assured by commanding $i_{dr}^{e*} = 0$. The real power flow can be used to regulate the dc voltage as illustrated by the controller block diagram in Figure 3. Since voltage-source pulse-width modulation (PWM) will be used, an additional PI loop is added whereby the commanded q-and d-axis rectifier voltages in the synchronous reference frame are obtained. Cross-coupling compensation terms can be added to the voltage command to account for q- and d-axis coupling [6]. However, ignoring these terms does not cause problems in this particular circuit since the axes are not tightly coupled. The PI gains used in this example are shown in Table II.

Table II. Controller gains.	
$K_{Piq} = 30\,\text{A/V}$	$K_{Pvq} = K_{Pvd} = 40\,\text{V/A}$
$K_{Iiq} = 100\,\text{A/V}\cdot\text{s}$	$K_{Ivq} = K_{Ivd} = 100\,\text{V/A}\cdot\text{s}$

Since the control is formulated in the synchronous reference frame, line synchronization is required for transformation of the measured currents to the synchronous reference frame and application of the commanded voltages. This is based on the measured voltages. In the example system low-pass filtered versions of the line-to-line voltages at the a-b-c terminals v_{ab} and v_{bc} were used to find the transformation terms

$$\cos\left(\theta_e + \phi_f + \frac{\pi}{6}\right) = \frac{\tilde{v}_{ab}}{a_f V_{LLp}} \qquad (3)$$
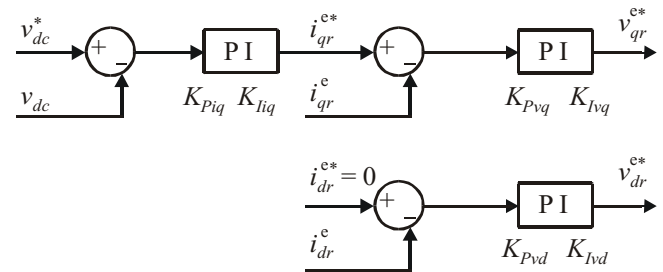

Figure 3. Active rectifier control.

$$\cos\left(\theta_e + \phi_f - \frac{\pi}{2}\right) = \frac{\tilde{v}_{bc}}{a_f V_{LLp}} \qquad (4)$$

where $\tilde{\ }$ represents filtered variables and V_{LLp} is the peak line-to-line voltage which can be observed using

$$V_{LLp} = \frac{2}{\sqrt{3}a_f}\sqrt{\tilde{v}_{ab}^2 + \tilde{v}_{bc}^2 + \tilde{v}_{ab}\tilde{v}_{bc}} \qquad (5)$$

In (3-5), a_f and ϕ_f are the low-pass filter attenuation and phase delay respectively which are related to the filter cut-off frequency f_c by

$$a_f = \left[1 + \left(\frac{f_e}{f_c}\right)^2\right]^{-\frac{1}{2}} \qquad (6)$$

$$\phi_f = -\tan^{-1}\left(\frac{f_e}{f_c}\right) \qquad (7)$$

By trigonometric identities, the terms (3-4) can be used to find cosine and sine functions of the synchronous reference frame position θ_e with any phase shift including the terms necessary to transform the load currents i_{al}, i_{bl}, and i_{cl} to the synchronous reference frame [6] yielding i_{ql}^e and i_{dl}^e needed for the control.

The next step in the control is to define duty cycles as

$$d_a = \frac{1}{2}\left[1 + m\cos(\theta_c) - \frac{m}{3}\cos(3\theta_c)\right] \qquad (8)$$

$$d_b = \frac{1}{2}\left[1 + m\cos\left(\theta_c - \frac{2\pi}{3}\right) - \frac{m}{3}\cos(3\theta_c)\right] \qquad (9)$$

$$d_c = \frac{1}{2}\left[1 + m\cos\left(\theta_c + \frac{2\pi}{3}\right) - \frac{m}{3}\cos(3\theta_c)\right] \qquad (10)$$

where m is the modulation index

$$m = \frac{2}{v_{dc}}\sqrt{\left(v_{qr}^{e*}\right)^2 + \left(v_{dr}^{e*}\right)^2} \qquad (11)$$

and θ_c is the converter angle which can be expressed as

$$\theta_c = \theta_e + \phi_v \qquad (12)$$

In (12), the voltage angle can be related to the commanded voltages by

$$\phi_v = -\tan^{-1}\left(\frac{v_{dr}^{e*}}{v_{qr}^{e*}}\right) \qquad (13)$$

In practice, trigonometric identities are used to obtain the terms in (8-10) as a function of the terms in (3-4). Once the duty cycles are obtained, they can be used for modulation according to the traditional sine-triangle method yielding the transistor signals for the converter [7].

B. Average-value Modeling

Two average-value models (assuming continuous conduction mode) were developed to facilitate the analysis presented herein. The first involves formulating the system in the synchronous reference frame. In this case, the PWM can be averaged by setting

$$\hat{v}_{qr}^e = v_{qr}^{e*} \qquad (14)$$

$$\hat{v}_{dr}^e = v_{dr}^{e*} \qquad (15)$$

where the $\hat{\ }$ symbol represents a fast-average or an average over one PWM cycle. On the dc side, the source is determined by setting

$$\hat{i}_{dc} = \frac{\hat{P}_e}{\hat{v}_{dc}} = \frac{3}{2\hat{v}_{dc}}\left(\hat{v}_{qr}^e\hat{i}_{qr}^e + \hat{v}_{dr}^e\hat{i}_{dr}^e\right) \qquad (16)$$

Note that (16) is an approximation since the average of products is replaced by the product of average variables. However, the results match the other average-value model described below and justify the approximation. The remainder of the circuit in Figure 2 consists of liner components and can be modeled by replacing the variables with their average-values. The equations for this circuit along with (14-16) were manually linearized in order to obtain the small-signal state-space model.

In the second average-value model, the equations were automatically linearized using the Advanced Continuous Simulation Language (ACSL) [7]. In this model, the circuit of Figure 2 was simulated in the source reference frame. The converter interface between the ac and dc system was averaged by assuming that the transistor signals T_a, T_b, and T_c are equal to their respective duty cycles listed in (8-10). Although this is a mix of *a-b-c* and *q-d* variables, the *a-b-c* variables do not involve states and are interfaced to the rest of the model in the following way. On the ac side, the average-value voltages can be calculated using

$$\begin{bmatrix} \hat{v}_{ar} \\ \hat{v}_{br} \\ \hat{v}_{cr} \end{bmatrix} = \frac{\hat{v}_{dc}}{3}\begin{bmatrix} 2 & -1 & -1 \\ -1 & 2 & -1 \\ -1 & -1 & 2 \end{bmatrix}\begin{bmatrix} d_a \\ d_b \\ d_c \end{bmatrix} \qquad (17)$$

These voltages are then transformed to the source reference frame. On the dc side, the average dc current is computed from

$$\hat{i}_{dc} = d_a\hat{i}_{ar} + d_b\hat{i}_{br} + d_c\hat{i}_{cr} \qquad (18)$$

The stability of the system can be assessed using the source and load impedances [4,5]. For the example system, an ac boundary was chosen between the filter capacitor and filter inductor (as indicated by the injection point in Figure 2) which defines source and load. In the steady-state, the source impedances are related to the voltages and currents in the arbitrary reference frame by

$$\begin{bmatrix} V_q \\ V_d \end{bmatrix} = \begin{bmatrix} Z_{qqS} & Z_{qdS} \\ Z_{dqS} & Z_{ddS} \end{bmatrix} \begin{bmatrix} I_{qs} \\ I_{ds} \end{bmatrix} \qquad (19)$$

On the load side, the admittance can be expressed in terms of the voltages and currents by

$$\begin{bmatrix} I_{qL} \\ I_{dL} \end{bmatrix} = \begin{bmatrix} Y_{qqL} & Y_{qdL} \\ Y_{dqL} & Y_{ddL} \end{bmatrix} \begin{bmatrix} V_q \\ V_d \end{bmatrix} \qquad (20)$$

Three criteria can be defined in order to determine stability by the combination of source impedance and load admittance [4].

$$ZY_{\infty 1} = \left\| Z_{qdS} \right\|_{\infty} \left\| Y_{qdL} \right\|_{1} \qquad (21)$$

$$ZY_{GG} = \left\| Z_{qdS} \right\|_{G} \left\| Y_{qdL} \right\|_{G} \qquad (22)$$

$$ZY_{\sigma\sigma} = \overline{\sigma}(Z_{qdS})\overline{\sigma}(Y_{qdL}) \qquad (23)$$

Therein, the $\overline{\sigma}$ is the largest singular of a matrix, and the infinity norm, the unity norm, and the G norm are defined by

$$\left\| Z_{qdS} \right\|_{\infty} = \max_i \left[\sum_j |Z_{ij}| \right] \qquad (24)$$

$$\left\| Y_{qdL} \right\|_{1} = \max_j \left[\sum_i |Y_{ij}| \right] \qquad (25)$$

$$\left\| A \right\|_{G} = \max \left(|a_{qq}|, |a_{qd}|, |a_{dq}|, |a_{dd}| \right) \qquad (26)$$

In (26), A represents a matrix with elements a_{ij} and can be impedance or admittance. Figure 4a shows three such criteria for the example system with parameters and operating conditions described above. For the example system, the impedances in (19-20) were computed using the average-value model which was linearized in ACSL. According to the criteria, the system will be stable if $ZY_{\infty 1} < 0.5$, or $ZY_{GG} < 0.25$, or $ZY_{\sigma\sigma} < 1$. From Figure 4a, it can be seen that only the $ZY_{\sigma\sigma}$ predicts system stability. However, this criterion is also the least restrictive (least conservative). Therefore, the criteria predict that the system is stable. If the system power is increased by decreasing the load resistance to $r_{load} = 35.1\,\Omega$ the stability criteria change as displayed in

Figure 4b. In this case, all criteria predict instability. Figure 4c shows the ACSL average-value simulation where the load resistance is stepped from $r_{load} = 67.6\,\Omega$ to $r_{load} = 35.1\,\Omega$. As predicted by the stability criteria, the system goes unstable when the power is increased.

The stability can also be assessed by creating a Nyquist plot of the Eigenvalues of the product of the source impedance and load admittance. This results in the 2x2 matrix

$$ZY = Z_{qdS} Y_{qdL} \qquad (27)$$

Figure 4d and 4e show the Nyquist plots for the stable and unstable case. In this example, it was determined through the linearized model that the system did not have any unstable open-loop poles. In that case, one CCW encirclement of the -1 point in the Nyquist plot would predict instability. As can be seen, the Nyquist plot predicts an instability when the load resistance is decreased.

III. AC IMPEDANCE MEASUREMENT

The small-signal source impedances and load admittances can be determined using series voltage disturbances or shunt current disturbances [4,5]. In this paper, injection of shunt currents was chosen. In a general form, an ac disturbance can be injected in the q-d reference frame as

$$i_{qi}^e = I_m \cos(\omega_s t) \cos(\phi_{inj}) \qquad (28)$$
$$i_{di}^e = I_m \cos(\omega_s t) \sin(\phi_{inj}) \qquad (29)$$

where I_m is the desired current injection amplitude, ϕ_{inj} is the injection angle and ω_s is the injection radian frequency which will be swept over a range of interest. By inverse transformation, the injected currents in machine variables become

$$i_{ai} = I_m \cos(\omega_s t) \cos(\omega_e t) \cos(\phi_{inj}) + \\ I_m \cos(\omega_s t) \sin(\omega_e t) \sin(\phi_{inj}) \qquad (30)$$

$$i_{bi} = I_m \cos(\omega_s t) \cos(\omega_e t - \tfrac{2\pi}{3}) \cos(\phi_{inj}) + \\ I_m \cos(\omega_s t) \sin(\omega_e t - \tfrac{2\pi}{3}) \sin(\phi_{inj}) \qquad (31)$$

$$i_{ci} = I_m \cos(\omega_s t) \cos(\omega_e t + \tfrac{2\pi}{3}) co s(\phi_{inj}) + \\ I_m \cos(\omega_s t) \sin(\omega_e t + \tfrac{2\pi}{3}) \sin(\phi_{inj}) \qquad (32)$$

When the currents are injected, the resulting voltage perturbations and source and load current perturbations at the injection frequency can be used to specifically calculate the source and load impedances [5]. For that a-b-c voltage at the injection terminal, the load and source currents must be transformed to the q-d synchronous reference frame and their components at the frequency of interest extracted. This is done at a desired injection frequency for several injection

a) criteria (stable case)

b) criteria (unstable case)

c) average-value model simulation

d) Nyquist plot (stable case)
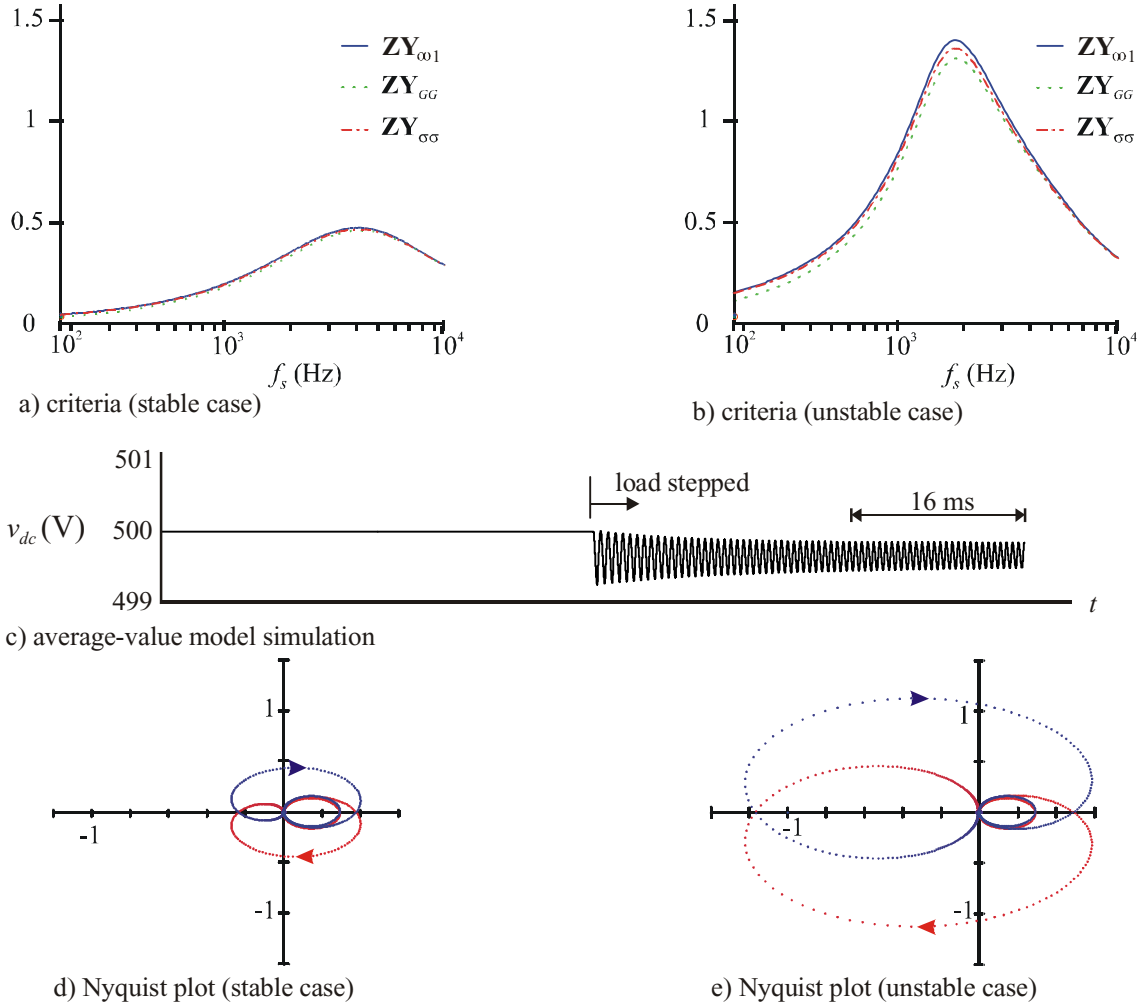
e) Nyquist plot (unstable case)

Figure 4. Stability criteria, average-value simulation and Nyquist plots.

angles in order to determine the impedances and admittances. For example the source impedance equation (19) can be re-written in the form

$$Ax = B \qquad (33)$$

where

$$B = \begin{bmatrix} \mathrm{Re}(V_{qq}) \\ \mathrm{Re}(V_{qd}) \\ \mathrm{Re}(V_{dq}) \\ \mathrm{Re}(V_{dd}) \\ \mathrm{Im}(V_{qq}) \\ \mathrm{Im}(V_{qd}) \\ \mathrm{Im}(V_{dq}) \\ \mathrm{Im}(V_{dd}) \end{bmatrix}, \quad x = \begin{bmatrix} \mathrm{Re}(Z_{qq}) \\ \mathrm{Re}(Z_{qd}) \\ \mathrm{Re}(Z_{dq}) \\ \mathrm{Re}(Z_{dd}) \\ \mathrm{Im}(Z_{qq}) \\ \mathrm{Im}(Z_{qd}) \\ \mathrm{Im}(Z_{dq}) \\ \mathrm{Im}(Z_{dd}) \end{bmatrix}$$

and A is the matrix required to satisfy (33) but is not written out here due to space constraints. The system of linear equations (33) is underdetermined system since it consists of

four unknowns and only two equations. To solve this problem (33) can be extended by combining two or more measurement results in one set of equations with each measurement corresponding to a unique angle ϕ_{inj}. A minimum of two measurements are necessary to obtain a solution. The solution represents a best fit to the data obtained from the current injection and can be automatically solved using a math processing software such as Matlab.

IV. PRACTICAL AC IMPEDANCE MEASUREMENT

The previous section described ideal currents that can be injected to determine the source impedance and load admittance. As a practical matter, this current injection can be accomplished by the three circuits shown in Figure 5.

A. Three-Phase Bridge Converter

The circuit in Figure 5a is a standard three-phase bridge converter. When applying this circuit for current injection, a current-regulated PWM method such as hysteresis

modulation or delta modulation [6] can be used to ensure the appropriate currents. By considering the injected currents of (30-32) and the general equation of power in the q-d reference frame (1), it can be seen that the average power at the point of injection is zero. This is the case since $v_d^e = 0$ and the power turns out to be a pure sinusoidal function at a frequency of ω_s. This means that it is possible to supply the bridge circuit from a pure capacitor source and regulate the capacitor voltage by adding an additional PI term to the commanded q-axis current. However, for the studies herein, a constant source of $v_c = 900\text{V}$ was used to obtain a set of results.

The advantage of the three-phase bridge converter is accurate control of the injected currents. However, this control means that the switching frequency of the inverter must be about 50 to 200 times the highest frequency component of the injected current. For this reason, the bridge converter circuit is recommended for low-voltage low-power systems where the appropriate transistors can be found.

B. Three-Phase Chopper Circuit

The second impedance measurement circuit introduced herein is the three-phase chopper topology shown in Figure 5b. This circuit is effectively and R-L load on the system where the load resistance can be effectively changed by switching the power transistors. The modulation of this circuit is a bit unconventional in that the transistors are switched using PWM, but the clock frequency is set to the desired injection frequency ω_s. The PWM duty cycles are then varied at the fundamental frequency with the desired injection angle using

$$d_{ac} = \frac{1}{2}\Big[1 + m_c \cos\big(\omega_e * t + \phi_{inj}\big)\Big] \qquad (34)$$

$$d_{bc} = \frac{1}{2}\left[1 + m_c \cos\left(\omega_e * t - \frac{2*\pi}{3} + \phi_{inj}\right)\right] \qquad (35)$$

$$d_{cc} = \frac{1}{2}\left[1 + m_c \cos\left(\omega_e * t + \frac{2*\pi}{3} + \phi_{inj}\right)\right] \qquad (36)$$

The injection can be viewed in the synchronous q-d reference frame as a switched R-L load with a varying impedance. For the study described below, the chopper circuit was operating with $R_c = 200\Omega$, $L_c = 1m\Omega$.

The primary advantage of the chopper circuit is that the switching frequency is set to the injected frequency and is very low compared to the bridge circuit introduced above. Therefore, this circuit is more suitable for medium-voltage systems where the transistor switching frequency is limited. The primary disadvantage is that the injected current will have considerable harmonics. However, this is somewhat filtered out by the system inductance and is mathematically removed by the demodulation process.

C. Wound Rotor Induction Machine

The final injection method presented herein is a wound rotor induction machine as shown in Figure 5c. In its application, the rotor circuit is first shorted and the machine is line-connected to the ac system allowing it to start and come up to synchronous speed. Then a set of dc currents is applied to the rotor windings from a low-power source. This ensures synchronous operation and the amount of dc current can be adjusted so that the reactive power is zero (the real power will be zero if there is no mechanical load placed upon the induction motor shaft). On top of the dc excitation is an ac excitation at the desired injection frequency. The injection is not that of (30-32), but of constant frequency nature as in (28-29) since the low-power supply is connected to the rotor of the machine and is therefore in the rotor reference frame. Furthermore, the phase angle of the rotor currents can be adjusted to obtain the injection angle ϕ_{inj}. The rotor injection can be accomplished by using a low-power three-phase bridge circuit or a low-power chopper circuit. For the studies on the example system, a three-phase bridge circuit was used. The induction motor parameters [6] are shown in Table III.

Table III. Parameters of the induction machine.	
$r_{sim} = 4.3785\Omega$	$l_{lsim} = 12.548mH$
$r_{rim} = 4.628793\Omega$	$l_{lrim} = 8.016mH$
$l_{mim} = 337.564mH$	$p = 2$

The biggest advantage is that this method can produce the same quality injection current as a three-phase bridge converter and be suitable for low- and medium- and high-voltage systems. The main disadvantage of this method is a custom design of a wound rotor induction machine.

D. Simulation Results

The three circuits described above were simulated as the current injection in the system shown in Figure 1. The frequency was swept from 180-Hz to 10,200-Hz and the source impedance and load admittance was extracted for each frequency. Figures 6a and 6b show the source impedances and load admittances determined from simulation using all three methods described above as well as the values calculated from the average-value model described above. Therein, the solid line denotes the average-value model prediction and the symbols correspond to the points predicted from the injection methods. As can be seen, all three methods predict the same impedance and match the ideal injection with such accuracy that there is little difference on the graph. These results were used to compute the three criteria mentioned above. Figure 6c shows the impedance criteria (which is the same as Figure 4a) with the results from the injection methods included. As can be seen, all methods determine the same ratio. Therefore, these simulation results

a) three phase bridge converter.

b) three phase chopper circuit.
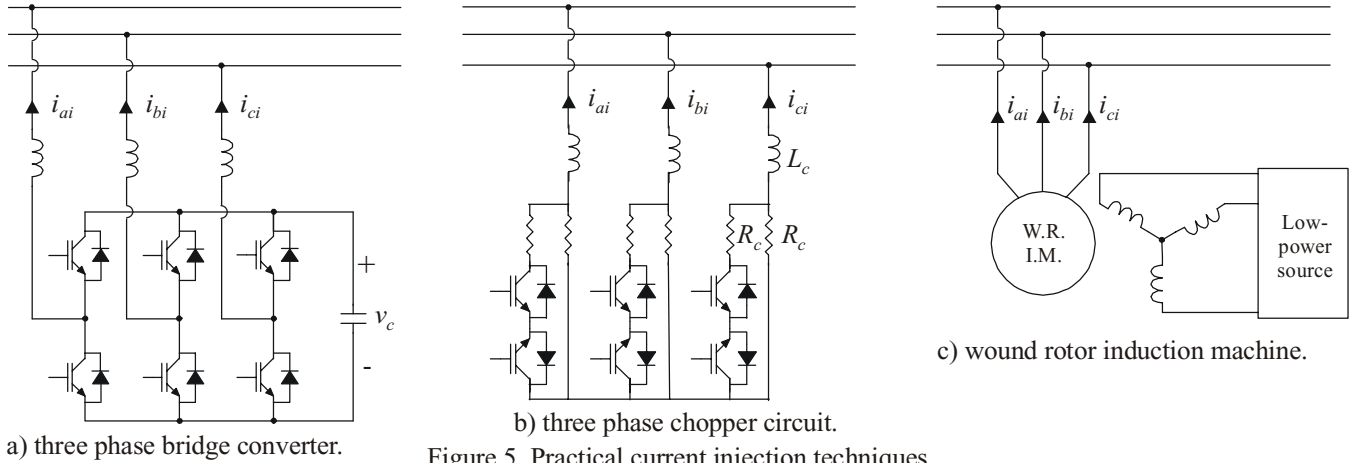
c) wound rotor induction machine.

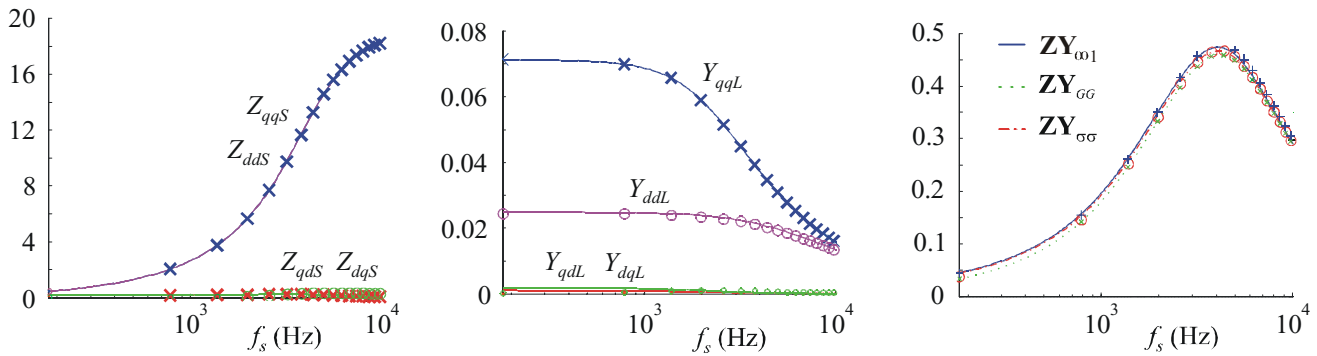Figure 5. Practical current injection techniques.

Figure 6. Source impedance, load admittance, and stability criteria as determined by the proposed injection methods.

demonstrate the effectiveness of the current injection methods proposed herein.

IV. CONCLUSION

Determination of source and load impedance is needed for prediction of stability in power electronics based systems. Past research has focused on the dc interface with some recent research on ac systems (as viewed in the q-d synchronous reference frame). This paper presents some additional ideas in the area of ac impedance injection. For ideal injection, a method of injecting currents at an arbitrary angle was described. Using this method, it is not necessary to inject currents specifically in the q- or d-axis. Instead, the injection angle can be arbitrary as long as at least two angles are used for each desired injection frequency. For practical current injection, this paper introduces three methods. The first two are power electronic circuits. For low-power systems, a standard three-phase bridge can be used. For higher power circuits, a novel chopper circuit was introduced which operates at a lower switching frequency. The third injection method amounts to using a wound-rotor induction machine so that the injected currents on the rotor side are already in the synchronous reference frame (assuming a dc bias is used to synchronize the rotor). A low-power bridge or chopper circuit can be used to switch currents into the rotor.

All three methods introduced were simulated on an example active rectifier system. It was shown that all methods predicted the same source impedance and load admittance and that these results agreed with the linearized small-signal model.

REFERENCES

1. R.D. Middlebrook, "Input Filter Considerations in Design and Application of Switching Regulators," *Proceedings of the IEEE Industry Applications Society Conference*, October 1976.

2. S.D. Sudhoff, K.A. Corzine, S.F. Glover, H.J. Hegner, and H.N. Robey Jr., "DC Link Stabilized Field Oriented Control of Electric Propulsion Systems," *IEEE Transactions on Energy Conversion*, volume 13, number 1, pages 27-33, March 1998.

3. S.D. Sudhoff, S.F. Glover, P.T. Lamm, D.H. Schmucker, and D.E. Delisle, "Admittance Space Stability Analysis of Power Electronic Systems," *IEEE Transactions on Aerospace and Electronic Systems*, volume 36, number 3, pages 965-973, July 2000.

4. M. Belkhayat, *Stability Criteria for AC Power Systems with Regulated Loads*, Ph.D. Dissertation, Purdue University, December 1997.

5. M. Belkhayat and M.L. Williams, "Impedance Extraction Techniques for Dc and Ac Systems," *Proceedings of the Naval Symposium on Electric Machines*, Philadelphia PA, December 2000.

6. P.C. Krause, O. Wasynczuk, and S.D. Sudhoff, *Analysis of Electric Machinery and Drive Systems*, IEEE Press, 2002.

7. K.A. Corzine and J.R. Baker, "Multi-Level Voltage-Source Duty-Cycle Modulation: Analysis and Implementation," *IEEE Transactions on Industrial Electronics*, volume 49, number 5, pages 1009-1016. October 2002.

8. *Advanced Continuous Simulation Language Reference Manual, Version 11*, MGA Software, 1995.

Yakov Familiant (S'00) received the BSEE degree from the Northwest Technological University, St. Petersburg, Russia, in 1995. He received the MSEE degree from the University of Wisconsin - Milwaukee in 2001 where he is presently pursuing a Ph.D. degree. His research interest include power electronics, electric machines, and digital control.

Keith A. Corzine (S'92-M'97) received the BSEE, MSEE, and Ph.D. degrees from the University of Missouri - Rolla in 1992, 1994, and 1997 respectively. He taught at the University of Wisconsin - Milwaukee from 1997 to 2004 and is now an Associate Professor at the University of Missouri - Rolla. His research interests include power electronics, motor drives, Naval ship propulsion systems, and electric machinery analysis.

Jing Huang (S'03) received the BSEE degree from Nan Chang University, Nan Chang, China, in 1997. She received her MSEE degree from the North China Electrical Power University in 2000 and is currently a Masters student at the University of Missouri - Rolla. Her research interests include multi-level converters, electrical machinery, and motor controls.

Mohamed Belkhayat received his Ph.D. in Electrical Engineering from Purdue University. He taught at the Naval Postgraduate School and the naval Academy. Currently, he is a research engineer with Northrop Grumman. His focus is in modeling, simulation and analysis of advanced naval power systems.